# Subventricular Zone Microstructure in Pediatric-Onset Multiple Sclerosis

Monica Margoni, MD, PhD,[1,2,3] Loredana Storelli, MSc, PhD,[1] Elisabetta Pagani, MSc,[1] Paolo Preziosa, MD, PhD,[1,2,4] Damiano Mistri, MSc,[1] Mor Gueye, MD,[1,2,4] Martina Rubin, MD,[1,2,4] Lucia Moiola, MD, PhD,[2] Massimo Filippi, MD,[1,2,3,4,5] and Maria Assunta Rocca, MD[1,2,4]

**Objective:** The aim of this study was to explore the microstructural dynamics of the subventricular zone (SVZ) with aging and their associations with clinical disability and brain structural damage in pediatric-onset multiple sclerosis (MS) patients.

**Methods:** One-hundred and forty-one pediatric-onset MS patients (67 pediatric and 74 adults with pediatric-onset) and 233 healthy controls (HC) underwent neurological and 3.0 T MRI assessment. Fractional anisotropy (FA) and mean diffusivity (MD) were extracted from the SVZ and the thalamus (as control region).

**Results:** In HC, SVZ FA was higher until age 40 then declined, whereas MD was lower until age 35 before rising (false discovery rate *p* value [pFDR] ≤ 0.008). Thalamic FA was higher until age 30 and then declined, whereas MD was higher until age 50 (pFDR ≤ 0.007). Pediatric MS patients showed significantly higher SVZ FA than pediatric HC (pFDR < 0.001), while adult patients showed no differences compared to adult HC (pFDR ≤ 0.724). Adult patients had lower thalamic FA and higher MD (pFDR < 0.001). Adults had lower SVZ FA and MD, but higher thalamic MD compared to pediatric patients (pFDR < 0.001). In pediatric MS, higher SVZ FA and MD were associated with higher white matter (WM) lesion volume (LV) and choroid plexus volume and lower brain and thalamic volumes (pFDR ≤ 0.047). In adult patients, higher SVZ MD associated with higher WM LV, lower brain volumes, and lower z-SDMT (pFDR≤0.019). Thalamic microstructural abnormalities were associated with more severe disability and brain damage in both groups (pFDR ≤ 0.018).

**Interpretation:** Our findings suggest that microstructural changes in the SVZ occur early in pediatric MS and are associated with brain structural damage but not with clinical impairment.

ANN NEUROL 2025;97:979–992

Pediatric-onset multiple sclerosis (MS) accounts for about 2 to 10% of the total MS cases.[1] Compared to adult-onset MS, patients with a pediatric-onset exhibit greater inflammatory activity early in the disease course but generally better functional recovery from clinical relapses.[2] It has been proposed that the younger age of these patients may offer protection through more effective brain repair capabilities, compensatory mechanisms, and plasticity, thereby limiting disability progression over time.[2,3] Thus, the study of these patients may provide a unique opportunity to understand the mechanisms underlying these processes.

Together with the subgranular zone in the hippocampal dentate gyrus, the subventricular zone (SVZ), located directly beneath the ependymal layer on the lateral wall of the lateral ventricles, harbors multipotent neural stem cells and progenitor cells.[4] The SVZ comprises an ependymal layer, a gap region, and an astrocytic ribbon,

View this article online at wileyonlinelibrary.com. DOI: 10.1002/ana.27180

Received Oct 2, 2024, and in revised form Dec 20, 2024. Accepted for publication Dec 21, 2024.

Address correspondence to Prof. Maria A. Rocca, Neuroimaging Research Unit, Division of Neuroscience, IRCCS San Raffaele Scientific Institute, Milan, Italy. E-mail: rocca.mara@hsr.it

From the [1]Neuroimaging Research Unit, Division of Neuroscience, IRCCS San Raffaele Scientific Institute, Milan, Italy; [2]Neurology Unit, IRCCS San Raffaele Scientific Institute, Milan, Italy; [3]Neurorehabilitation Unit, IRCCS San Raffaele Scientific Institute, Milan, Italy; [4]Vita-Salute San Raffaele University, Milan, Italy; and [5]Neurophysiology Service, IRCCS San Raffaele Scientific Institute, Milan, Italy

 

and it is separated from the caudate nucleus and the striatum by a myelin layer. Within this region, 3 distinct cell types (type A, type B, and type C) are organized in a specific pattern: type A cells are located nearest to the ependymal layer, type B cells form the astrocytic ribbon, and type C cells are placed closer to the myelin layer and the striatum.[5] While most information on SVZ function comes from experimental studies, evidence in humans suggests the persistence of stem cell activity in the adult brain.[6] However, the cellular organization of SVZ undergoes changes during human brain development, diminishing its functional capacity from infancy to adulthood.[7–9] Although the proliferative and migratory capacity of SVZ cells in vivo remains debated,[6,7] recent findings suggest that under normal and injury conditions, the adult human SVZ can produce mature astrocytes.[10] Moreover, post-mortem studies have identified mature and immature oligodendrocytes and oligodendrocyte precursor cells in chronic MS lesions, indicating mobilization of SVZ-derived progenitors mainly to periventricular lesions.[11] In experimental models of MS, SVZ-derived cells have also been implicated in remyelination through various mechanisms.[12–14] Finally, accumulating evidence suggests that the SVZ may exert other functions via secretion of soluble growth factors, release of neuroprotective molecules, and modulation of microglia functions.[15]

So far, only a few MRI studies have applied quantitative MRI techniques, such as diffusion tensor imaging (DTI), to evaluate microstructural abnormalities of the SVZ and their clinical relevance in adult patients with MS, by showing similar fractional anisotropy (FA) and higher mean diffusivity (MD) compared to healthy controls (HC) and an association with clinical and cognitive disability.[15,16] Whether this structure might be affected from the earliest phases of the disease, when stem cell activity of the SVZ is likely to be more relevant, has not been investigated. Here, we hypothesized that in the early stages of MS, there might be compensatory mechanisms related to the activation of the SVZ cells that could disappear as disease duration increases.

To test our hypothesis, we characterized SVZ microstructural features in a large cohort of pediatric-onset MS patients. For a proper interpretation of disease-related modifications of this structure with age, we also defined the physiological modifications of microstructural features of the SVZ in HC across a wide age range. For a more comprehensive understanding of our findings, given the recently described choroid plexus-SVZ regulatory axis,[17] in which choroid plexus could regulate the stem cell properties of the SVZ through the secretion of small extracellular vesicles,[17] we evaluated the association between SVZ and choroid plexus volume, in addition to usual MRI measures of brain structural damage (T2-hyperintense white matter [WM] lesions and atrophy). Finally, to explore the clinical relevance of SVZ abnormalities, we assessed the relationship with clinical disability (Expanded Disability Status Scale [EDSS] score and Symbol Digit Modalities Test [SDMT]).

## Methods

### Standard Protocol Approvals, Registrations, and Patient Consents

Approval was received from the local ethical standards committee on human experimentation, and written informed consent was obtained from all participants and their parents prior to study enrollment.

### Participants

In this cross-sectional, retrospective, observational study, we included 141 consecutive relapsing–remitting pediatric-onset MS (hereafter defined as pediatric MS if aged <18 years [n = 67] and adults with pediatric-onset MS if aged ≥18 years [n = 74]), diagnosed according to the 2017 McDonald criteria and fulfilling the dissemination in space and time criteria.[18] These patients are part of ongoing prospective cohorts of patients recruited at San Raffaele Hospital, Milan, Italy. Patients had to be relapse- and steroid-free for at least 1 month prior to clinical and MRI assessment. Whenever needed, appropriate testing was performed to exclude leukodystrophies and myelin oligodendrocyte glycoprotein antibody-associated disease. Exclusion criteria were concomitant therapy with antidepressants, psychoactive drugs, or a history of other primary neurological or psychiatric disorders in addition to MS. Two hundred and 33 HC (22 pediatric HC and 211 adult HC), aged between 8 and 50 years, with no previous history of neurological dysfunction and a normal neurological examination served as the control group.

### Clinical Assessment

On the day of MRI acquisition, MS patients underwent a complete neurologic evaluation, with rating of the EDSS score and recording of ongoing disease-modifying treatments (DMTs). The clinical assessment was performed by an experienced neurologist, unaware of the MRI results. Within 48 hours from the MRI acquisition, experienced neuropsychologists administered SDMT to assess information processing speed. A z-score was determined according to age-appropriate normative data.[19,20]

### MRI Acquisition

Using a 3.0 T Philips Intera MR scanner with 8-channel head coil (Philips Medical System), the following sequences of the brain were acquired from all subjects

during a single session: (1) dual-echo turbo spin echo (repetition time [TR] = 2,599 milliseconds [msec]; echo time [TE] = 16–80 msec; flip angle = 90°; matrix = 256 × 256; field of view [FOV] = 240 millimiters [mm]$^2$; echo train length [ETL] = 6; 44 contiguous axial slices, 3 mm thick); and (2) 3-dimensional (3D) T1-weighted fast field echo (TR = 25 msec; TE = 4.6 msec; flip angle = 30°; matrix = 256 × 256; FOV = 230 mm$^2$; 220 contiguous axial slices, 0.8 mm thick); (3) pulsed-gradient spin echo echo-planar imaging (TR/TE 8775/58 msec, matrix size = 112 × 88, FOV = 240 × 231 mm$^2$, 55 contiguous, 2.3 mm thick axial slices) with SENSE (acceleration factor = 2) and diffusion gradients applied in 35 non-collinear directions. Two optimized b factors were used for acquiring diffusion weighted images (b1 = 0, b2 = 900 sec/mm$^2$).

### Conventional MRI Analysis

In all subjects, T2-hyperintense WM lesions were identified on the dual-echo sequence using a local thresholding segmentation technique (Jim 8, Xinapse Systems).

Normalized brain volume (NBV) was measured on the 3D T1-weighted sequence using the FSL-SIENAx2 software, after T1-hypointense lesion refilling.[21] From the same tool, the thalamic, caudate, and ventricular segmentations were also obtained, together with their normalized volumes.[22] Given its similar anatomical localization to the SVZ, we defined the thalamus as the control region. Lateral ventricle volume was measured after manual editing of the ventricular cerebrospinal fluid (CSF) map.

### Pre-Processing of Diffusion-Weighted Imaging

Pre-processing of diffusion-weighted images included correction for off-resonance and eddy current-induced distortions and movements using the Eddy tool in the FSL library.[23] A b0 image with reversed polarity of gradients was not available; therefore, an undistorted b0 image was simulated[24] from the 3D T1-weighted sequence to be used for distortion correction. The diffusion tensor was estimated by linear regression, and maps of FA and MD were derived.

### Identification of the SVZ and Control Thalamic Region

For each subject lateral ventricles, caudate and thalamus were already segmented using the automated tool FIRST from FSL Library.[22] Subsequently, we identified the intersection regions between lateral ventricles and 2 neighboring structures: caudate and thalamus (Fig 1). We identified the region of intersection between the caudate and the lateral ventricles as the SVZ. We selected the other region bordering the thalamus, since this area is likely to comprise an identical relative proportion of voxels belonging to the lateral ventricles and to the respective subcortical nucleus without identifying any specific anatomical areas, thus acting as potential control region to check only for possible partial volume systematic errors, as suggested in a previous study.[25] By using an image dilation morphological operation, as implemented in MATLAB® (version R2017a), 2 image masks of the intersection between the dilated lateral ventricle and the corresponding portion of either the caudate and the thalamus were obtained, including the voxels that were comprised in a laminar volume surrounding the ventricle with a thickness of 3 mm on the 3D T1-weighted sequence. These segmented areas defined the region of interest (ROI) that were superimposed on the reconstructed DTI-derived measures (FA and MD), after co-registering T1-weighted volume on FA maps. We then applied a threshold of 50% on the co-registered probability SVZ masks, excluding voxels below this value from the analysis, to increase the probability of including voxels that truly belong to the SVZ region. For each subject, the resulting images were visually assessed by 2 trained neurologists (P.P., M.M.) to exclude misregistration or erroneous ROI identification. From these ROI, mean MD and FA values were calculated for each individual.

### Segmentation and Quantification of Choroid Plexus Volume

The choroid plexuses of the lateral ventricles were manually segmented in the axial planes of the 3D T1-weighted sequence using a local thresholding segmentation technique (Jim 8, Xinapse Systems) by 2 experienced raters (M.M. and M.G.) and their volume was calculated as previously described.[26] The choroid plexuses of the third and fourth ventricles were not included in the analysis, given their inconstant visualization.[26] The volume of choroid plexuses and lateral ventricles were multiplied by V scaling (derived from the SIENAx, as a measure of head size) to obtain the corresponding normalized values.

### Statistical Analysis

Demographic and clinical features were compared between HC and pediatric-onset MS using Fisher's exact, Mann–Whitney U tests or linear models, as appropriate. Age- and sex-adjusted linear models were performed to assess differences in MRI features between HC and MS patients.

To estimate FA and MD expected lifespan trajectories in the SVZ and the thalamic region, we fitted linear regression models to HC data. Sex, age and age squared were included as fixed effects according to Akaike information criterion. First-order derivative (estimated slope) of each model was evaluated across ages (steps of 5 years) to assess the rates of DTI values changes. For each model,

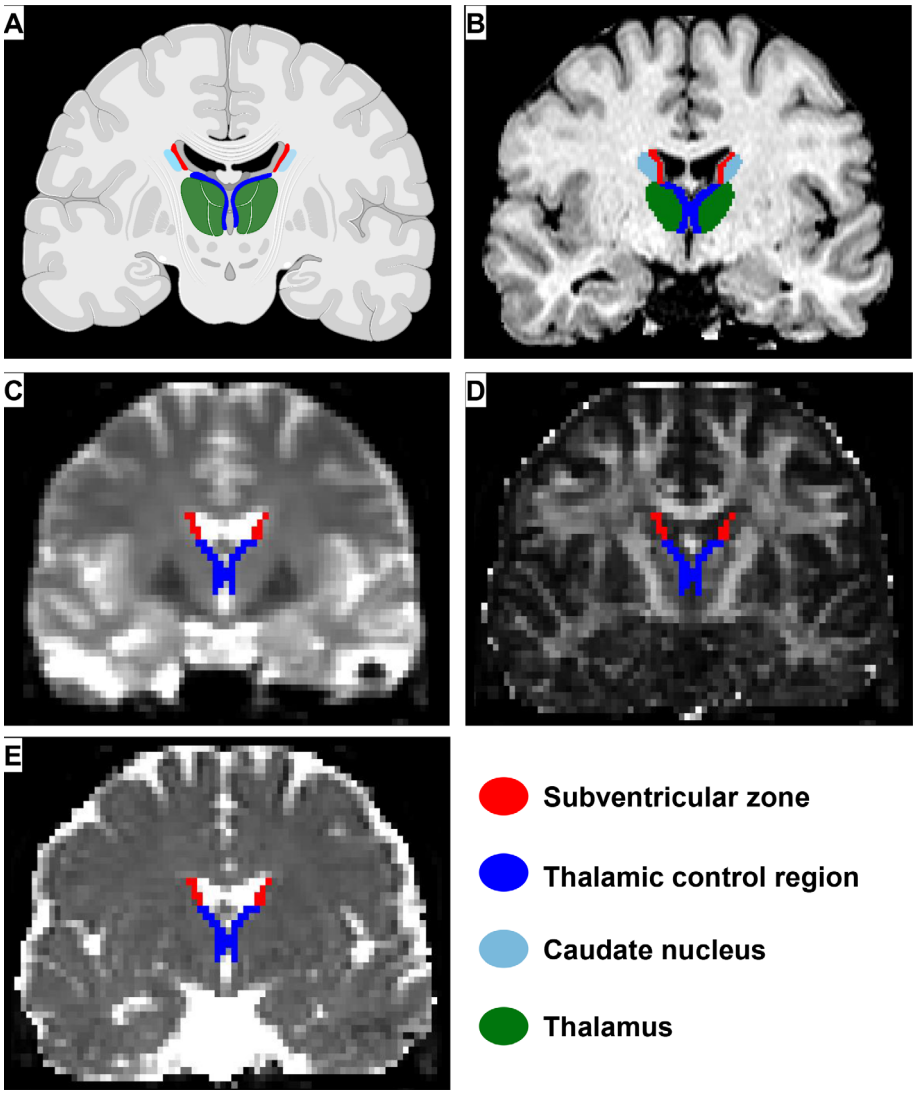


**FIGURE 1: Identification of the subventricular zone and thalamic control region and methodological workflow. (A) Anatomical localization of the subventricular zone (red) located in-between the caudate nucleus (light blue) and the CSF; in blue the band of the thalamus (green) close to the CSF which serves as region of control (created with biorender.com). (B) Coronal plane of T1-weighted sequence showing the thalamus and caudate nucleus with superimposed the created masks for the subventricular zone and thalamic region. (C) The masks created on T1-weighted sequence were co-registered to the b0 image and then superimposed on FA (D) and MD (E) maps. See text for further details. CSF = cerebrospinal fluid; FA = fractional anisotropy; MD = mean diffusivity [Color figure can be viewed at www.annalsofneurology.org]**

we tested the nullity of the slope across ages (ie, the change of the trend for each trajectory).

Estimated parameters from the described models were then used to convert DTI values measured in pediatric MS and adults with pediatric-onset MS to z-scores, which are relative to sex- and age-corrected values from HC. In particular, they represent a standardized measure of deviation from the sex- and age-specific expected values in the HC' population. We assessed (testing the nullity, that is, healthy population reference value, of the estimated means) and compared z-scores in patients with pediatric and pediatric-onset MS by linear models. Then, we ran multiple linear regression models to investigate the association of SVZ and thalamic region DTI z-scores with clinical and MRI metrics in pediatric MS patients and adults with pediatric-onset MS.

Benjamini-Hochberg false discovery rate (FDR) correction was carried out to account for the overall number of tests performed, for each analysis separately.

Software R (version 4.2.2) was used for computations. All $p$ values <0.05 were deemed statistically significant.

## Results

### *Demographic, Clinical and Conventional MRI Findings*

Table 1 summarizes the main demographic, clinical and MRI features in HC and MS patients.

**TABLE 1. Main Demographic, Clinical, and MRI Characteristics of Healthy Controls and Pediatric-Onset Multiple Sclerosis Patients**

| Variable | | Pediatric HC (n = 22) | Pediatric MS (n = 67) | *p*-Value (pFDR) | Adult HC (n = 211) | Adults with Pediatric-Onset MS (n = 74) | *p*-Value (pFDR) |
|---|---|---|---|---|---|---|---|
| Sex | Male (%) | 13 (59) | 25 (37) | 0.073 | 113 (54) | 45 (61) | 0.279 |
| | Female (%) | 9 (41) | 42 (63) | (0.292) | 98 (46) | 29 (39) | (0.558) |
| Median age (IQR), (range) (years) | | 14.6 (12.0; 16.2), (8.5; 17.9) | 15.5 (14.5;16.9), (7.6; 17.9) | 0.633 (0.633) | 27.0 (23.7; 35.1), (18.1; 49.8) | 28.8 (22.6; 37.3), (18.1; 48.8) | 0.171 (0.513) |
| Median age at onset (IQR), (range) (years) | | - | 13.6 (11.9; 15.1), (5.3; 17.5) | - | - | 15.6 (13.9;16.9), (8.0; 18.7) | - |
| Median disease duration (IQR) (years) | | - | 1.4 (0.6; 2.6) | - | | 13.3 (9.0; 22.0) | - |
| Median EDSS score (IQR) | | - | 1.5 (1.0; 2.0) | - | | 1.5 (1.0; 4.0) | - |
| Median z-SDMT score (IQR) | | - | −0.07 (−0.68; 0.31) | - | | −0.93 (−1.64; 0.01) | - |
| Patients receiving DMTs (%) | | - | 54 (81) | - | | 57 (77) | - |
| Median brain T2-hyperintense WM LV[a] (IQR) (mL) | | 0.0 (0.0; 0.1) | 3.7 (2.0; 8.1) | **<0.001 (<0.001)** | 0.0 (0.0; 0.2) | 5.2 (2.3; 11.8) | **<0.001 (<0.001)** |
| EM (SE) | NBV (mL) | 1725 (15) | 1,678 (10) | **0.001 (0.008)** | 1,646 (6) | 1,576 (8) | **<0.001 (<0.001)** |
| | Normalized thalamic volume (mL) | 23.03 (0.40) | 22.15 (0.27) | **0.002 (0.015)** | 22.94 (0.16) | 20.47 (0.23) | **<0.001 (<0.001)** |
| | Normalized caudate volume (mL) | 10.81 (0.26) | 10.46 (0.18) | 0.036 (0.216) | 10.04 (0.10) | 9.39 (0.14) | **<0.001 (<0.001)** |
| | Normalized CP volume (mL) | 2.01 (0.18) | 2.91 (0.14) | **<0.001 (<0.001)** | 2.44 (0.06) | 2.76 (0.09) | **<0.001 (0.002)** |
| | Normalized lateral ventricle volume (mL) | 14.34 (1.60) | 21.87 (1.42) | **0.002 (0.003)** | 19.99 (1.29) | 32.69 (1.80) | **<0.001 (<0.001)** |

Comparisons performed by Fisher's exact test (sex) and Mann–Whitney test (age, WM lesion volumes). Age- and sex-adjusted linear models were performed for MRI variables. Age-, sex-, NBV, and lateral ventricle volume-adjusted linear regression model was performed for normalized choroid plexus volume. Bold values denote statistical significance ($p < 0.05$).

CP = choroid plexus; DMT = disease modifying therapy; EDSS = Expanded Disability Status Scale; EM = estimated mean; HC = healthy controls; IQR = interquartile range; LV = lesion volume; mL = milliliter; MS = multiple sclerosis; NBV = normalized brain volume; pFDR = false discovery rate *p* value; SDMT = Symbol Digit Modalities Test; SE = standard error; WM = white matter.

[a]T2-hyperintense white matter lesion volume was log transformed for the analyses.

Compared to pediatric HC, pediatric MS patients had significantly higher brain T2-hyperintense WM LV and choroid plexus volume (all FDR *p* value [pFDR] <0 .001) as well as lower NBV and normalized thalamic volumes (pFDR ≤ 0.015). No significant differences in terms of age, sex, and caudate volume were observed (pFDR ≥ 0.216).

Compared to adult HC, adults with pediatric-onset MS had significantly higher brain T2-hyperintense WM LV and choroid plexus volume (pFDR ≤ 0.002) as well as lower NBV, normalized thalamic and caudate volumes (all pFDR < 0.001). No significant differences in terms of age and sex were observed (pFDR ≥ 0.513).

### *SVZ and Thalamic Control Region DTI Trajectories in HC*

In HC, FA values were significantly higher in the SVZ up to the age of 40 years, and in the thalamus up to 30 years (pFDR ≤ 0.007). Subsequently, a significant lowering was observed in both structures. Conversely, MD values were significantly lower in the SVZ up to the age of 35 years (pFDR ≤ 0.001) and then progressively higher until the age of 50 years. In the thalamus, MD values were higher until age 50 (pFDR ≤ 0.004) (Fig 2, Table 2).

### *SVZ and Thalamic Control Region in Pediatric-Onset MS*

Compared to pediatric HC, SVZ FA values were significantly higher in pediatric MS patients (pFDR < 0.001), whereas no significant differences were observed for SVZ MD (pFDR = 0.550). No significant differences were observed in both metrics in adults with pediatric-onset MS compared to adult HC (pFDR = 0.724 and $P = 0.302$).

Compared to pediatric HC, pediatric MS patients showed no differences in both thalamic FA and MD (pFDR = 0.101 and pFDR = 0.550); whereas, compared to adult HC, adults with pediatric-onset MS showed significantly lower thalamic FA and higher thalamic MD (all pFDR < 0.001).

Compared to pediatric MS patients, adults with pediatric-onset MS had significantly lower SVZ FA and MD (pFDR < 0.001), as well as higher thalamic MD (pFDR<0.001) (Table 3, Fig 3).

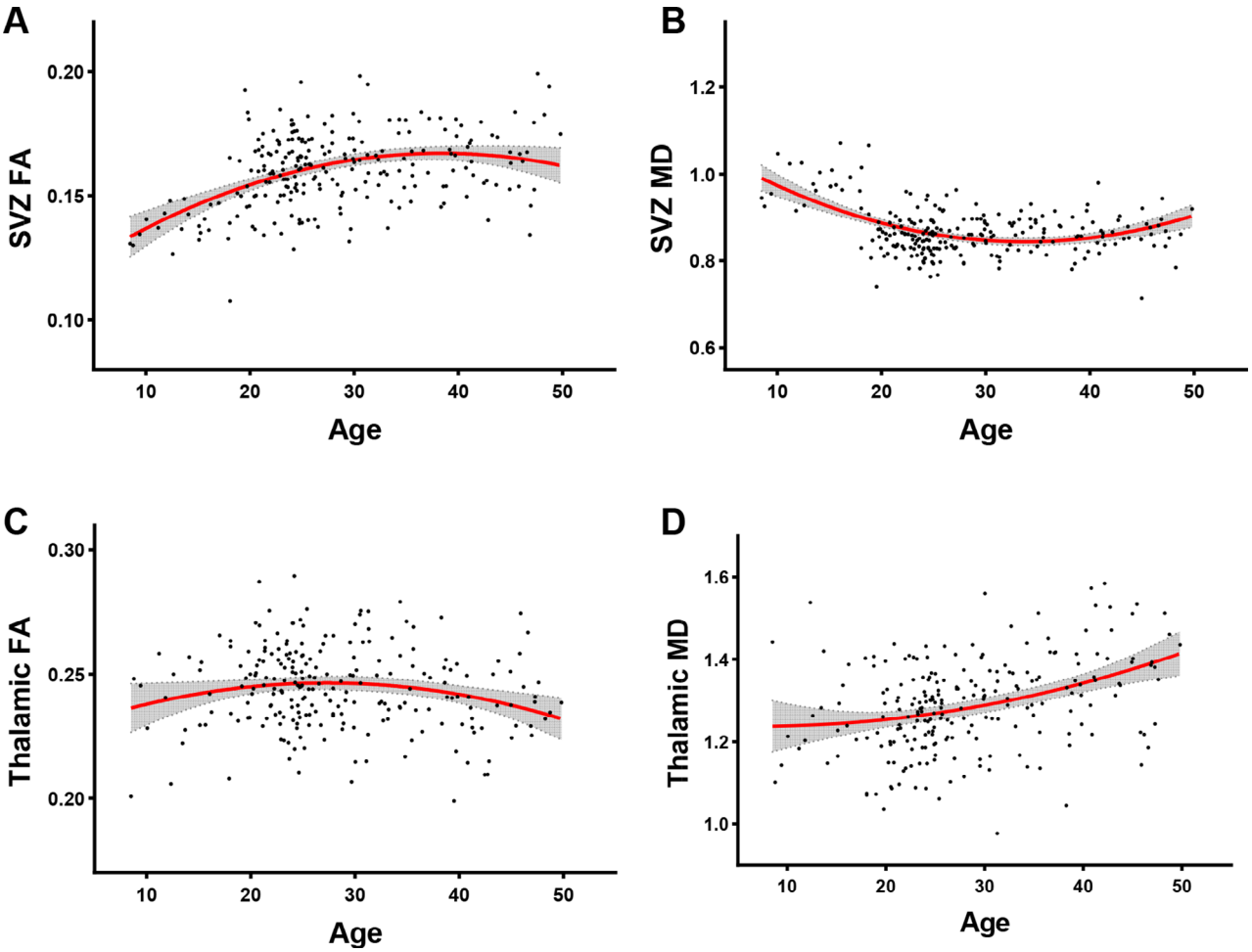


**FIGURE 2: Estimated sex-adjusted DTI metrics lifespan trajectories in the subventricular zone and thalamic region of healthy controls. The figure shows mean estimated sex-adjusted DTI values (solid lines with 95% shaded CIs) in the (A, B) subventricular zone and (C, D) thalamus. CI = confidence interval; FA = fractional anisotropy; DTI = diffusion tensor imaging; MD = mean diffusivity; SVZ = subventricular zone [Color figure can be viewed at www.annalsofneurology.org]**

**TABLE 2. Mean Estimated DTI Values Across Ages (Steps of 5 Years) from Sex-Adjusted Lifespan Trajectories in the Subventricular Zone and Thalamus of Healthy Controls**

| Parameter | Age (years) | Estimated Mean (SE) | Estimated Slope (SE) [$\times 10^{-3}$] | *p*-Value (pFDR)[a] |
|---|---|---|---|---|
| SVZ FA | 5–10 | 0.134 (0.004) | 2.294 (0.001) | **<0.001 (<0.001)** |
| | 10–15 | 0.142 (0.003) | 1.915 (0.001) | **<0.001 (<0.001)** |
| | 15–20 | 0.152 (0.002) | 1.536 (0.001) | **<0.001 (<0.001)** |
| | 20–25 | 0.158 (0.001) | 1.157 (0.001) | **<0.001 (<0.001)** |
| | 25–30 | 0.162 (0.001) | 0.779 (0.001) | **<0.001 (0.001)** |
| | 30–35 | 0.166 (0.001) | 0.400 (0.001) | **<0.001 (0.005)** |
| | 35–40 | 0.167 (0.002) | 0.021 (0.001) | 0.710 (0.710) |
| | 40–45 | 0.166 (0.002) | −0.357 (0.001) | **0.030** (0.050) |
| | 45–50 | 0.165 (0.003) | −0.736 (0.001) | **0.001 (0.002)** |
| SVZ MD | 5–10 | 0.986 (0.015) | −11.816 (0.006) | **<0.001 (<0.001)** |
| | 10–15 | 0.949 (0.011) | −9.523 (0.006) | **<0.001 (<0.001)** |
| | 15–20 | 0.902 (0.006) | −7.230 (0.006) | **<0.001 (<0.001)** |
| | 20–25 | 0.871 (0.005) | −4.937 (0.006) | **<0.001 (<0.001)** |
| | 25–30 | 0.855 (0.005) | −2.644 (0.006) | **0.001 (0.004)** |
| | 30–35 | 0.845 (0.005) | −0.351 (0.006) | 0.339 (0.340) |
| | 35–40 | 0.848 (0.006) | 1.941 (0.005) | **0.004 (0.008)** |
| | 40–45 | 0.861 (0.007) | 4.233 (0.005) | **<0.001 (<0.001)** |
| | 45–50 | 0.884 (0.010) | 6.526 (0.005) | **<0.001 (<0.001)** |
| Thalamic FA | 5–10 | 0.237 (0.004) | 2.294 (0.001) | **<0.001 (<0.001)** |
| | 10–15 | 0.240 (0.003) | 1.915 (0.001) | **<0.001 (<0.001)** |
| | 15–20 | 0.244 (0.002) | 1.536 (0.001) | **<0.001 (0.001)** |
| | 20–25 | 0.246 (0.001) | 1.157 (0.001) | **0.004 (0.007)** |
| | 25–30 | 0.246 (0.001) | 0.779 (0.001) | 0.432 (0.432) |
| | 30–35 | 0.246 (0.001) | 0.400 (0.001) | **0.002 (0.004)** |
| | 35–40 | 0.243 (0.001) | 0.021 (0.001) | **<0.001 (0.001)** |
| | 40–45 | 0.240 (0.002) | −0.357 (0.001) | **<0.001 (<0.001)** |
| | 45–50 | 0.236 (0.003) | −0.736 (0.001) | **<0.001 (<0.001)** |
| Thalamic MD | 5–10 | 1.234 (0.030) | 0.213 (0.013) | 0.189 (0.189) |
| | 10–15 | 1.242 (0.022) | 1.167 (0.012) | **0.001 (0.010)** |
| | 15–20 | 1.251 (0.013) | 2.120 (0.013) | **<0.001 (<0.001)** |
| | 20–25 | 1.263 (0.010) | 3.074 (0.013) | **<0.001 (<0.001)** |
| | 25–30 | 1.277 (0.010) | 4.027 (0.013) | **<0.001 (<0.001)** |
| | 30–35 | 1.299 (0.011) | 4.981 (0.013) | **<0.001 (<0.001)** |
| | 35–40 | 1.328 (0.012) | 5.935 (0.012) | **<0.001 (<0.001)** |
| | 40–45 | 1.352 (0.014) | 6.888 (0.011) | **<0.001 (<0.001)** |
| | 45–50 | 1.397 (0.021) | 7.842 (0.012) | **<0.001 (<0.001)** |

Note: The first-order derivative (estimated slope) of the model is also shown, to assess DTI values change rate. Linear regression model including sex, age and age square as fixed effects, according to Akaike information criterion.

DTI = diffusion tensor imaging; FA = fractional anisotropy; pFDR = false discovery rate *p* value; MD = mean diffusivity; SE = standard error; SVZ = subventricular zone.

[a]The *p* values of the test for the nullity of the slope. FDR correction (Benjamini-Hochberg procedure) was applied to account for the overall number of tests. Bold values denote statistical significance ($p < 0.05$).

**TABLE 3. Mean Estimated DTI Z-Scores of the Subventricular Zone and Thalamic Region in Pediatric-Onset Multiple Sclerosis Patients and Healthy Controls**

| Parameter | Pediatric HC<br>Mean (SD) | Pediatric MS<br>Mean (SD) | Pediatric MS vs Pediatric HC<br>*p*-Value (pFDR)[a] | Adult HC<br>Mean (SD) | Adults with Pediatric-Onset MS<br>Mean (SD) | Adults with Pediatric-Onset MS vs Adult HC<br>*p*-Value (pFDR)[a] | Adults with Pediatric-Onset MS vs Pediatric MS<br>*p*-Value (pFDR)[a] |
|---|---|---|---|---|---|---|---|
| **SVZ FA** | −3.368 (1.256) | 2.275 (1.603) | **<0.001 (<0.001)** | 0.233 (1.909) | 0.133 (2.583) | 0.724 (0.724) | **<0.001 (<0.001)** |
| **SVZ MD** | 4.237 (1.688) | 4.768 (2.049) | 0.275 (0.550) | −0.442 (1.570) | 0.529 (2.741) | 0.079 (0.302) | **<0.001 (<0.001)** |
| **Thalamic FA** | −2.030 (5.573) | −4.615 (5.956) | **0.025** (0.101) | 0.212 (5.009) | −5.710 (6.564) | **<0.001 (<0.001)** | 0.255 (0.750) |
| **Thalamic MD** | −0.481 (2.792) | 0.378 (3.191) | 0.262 (0.550) | 0.050 (2.508) | 5.286 (5.956) | **<0.001 (<0.001)** | **<0.001 (<0.001)** |

FA = fractional anisotropy; DTI = diffusion tensor imaging; pFDR = false discovery rate *p* value; HC = healthy controls; MD = mean diffusivity; MS = multiple sclerosis; SD = standard deviation; SVZ = subventricular zone.

[a]The *p* values of the test for the nullity (ie, healthy population expected value) of the mean estimated z-scores in each group and of significant between-group comparisons are reported (linear models). FDR correction (Benjamini-Hochberg procedure) was applied to account for the overall number of tests. Bold values denote statistical significance ($p < 0.05$).

### *Analysis of Associations*

In pediatric MS patients, higher SVZ FA was significantly associated with higher brain T2-hyperintense WM LV ($\beta = 0.006$; pFDR = 0.047) and higher normalized choroid plexus volume ($\beta = 0.005$; pFDR = 0.004). Higher SVZ MD was significantly associated with higher brain T2-hyperintense WM LV ($\beta = 0.038$; pFDR = 0.019), as well as lower normalized brain and thalamic volumes ($\beta = -0.889$; pFDR < 0.001 and $\beta = -0.410$; pFDR = 0.003). Lower thalamic FA and higher thalamic MD values were significantly associated with higher T2-hyperintense WM LV and choroid plexus volume as well as lower NBV, normalized thalamic and caudate volumes (FA: $\beta$ ranging from −0.016 to 0.566, pFDR ≤ 0.007; MD: $\beta$ ranging from −1.853 to 0.152; pFDR ≤ 0.013) (Table 4).

In adults with pediatric-onset MS, no associations were observed between SVZ FA and the other investigated variables; whereas, higher SVZ MD significantly associated with higher brain T2-hyperintense WM LV ($\beta = 0.026$; pFDR = 0.001) as well as lower z-SMDT score ($\beta = -0.302$; pFDR = 0.019), normalized brain ($\beta = -0.378$; pFDR = 0.002), thalamic ($\beta = -0.447$; pFDR = 0.003), and caudate volumes ($\beta = -0.398$; pFDR = 0.016). Lower thalamic FA and higher thalamic MD values were significantly associated with higher EDSS score, T2-hyperintense WM LV, and normalized choroid plexus volume, as well as lower z-SDMT, NBV, normalized thalamic and caudate volumes both in pediatric MS and adults with pediatric-onset MS (FA: β ranging from −0.381 to 0.604, pFDR ≤ 0.018; MD: β ranging from −1.189 to 0.330; pFDR ≤ 0.014) (Table 4).

## Discussion

By evaluating a large cohort of pediatric-onset MS patients and HC across a wide age range, this study provided new insights into the trajectories of DTI metrics occurring with aging in the SVZ and how the disease may impact this region compared to a similar anatomical structure, namely the thalamus, in pediatric-onset MS.

The analysis of HC revealed that both FA and MD varied with aging in both the SVZ and control thalamic region. Specifically, FA in the SVZ gradually increased until mid-age, followed by a slight decrease. In contrast, MD values in the SVZ significantly decreased until around age 35, after which it began to increase. These findings may be explained by different underlying physiological processes (Fig 4). The gradual increase of FA and decrease of MD observed in the SVZ could both be attributed to ongoing developmental processes, such as myelination, axonal growth, synaptic pruning,[27,28] occurring during childhood until early adulthood. Notably, steeper slopes were observed in the first 2 decades for both DTI metrics. Indeed, the SVZ is considered a critical area for the potential stemness, where neural stem cells and neural progenitor cells proliferate and differentiate, particularly in early development.[7,8] This active neurogenic environment results in a denser microstructure, with increased cellularity and the proliferation of glial cells and precursors,[29] leading to more restricted diffusion of water molecules

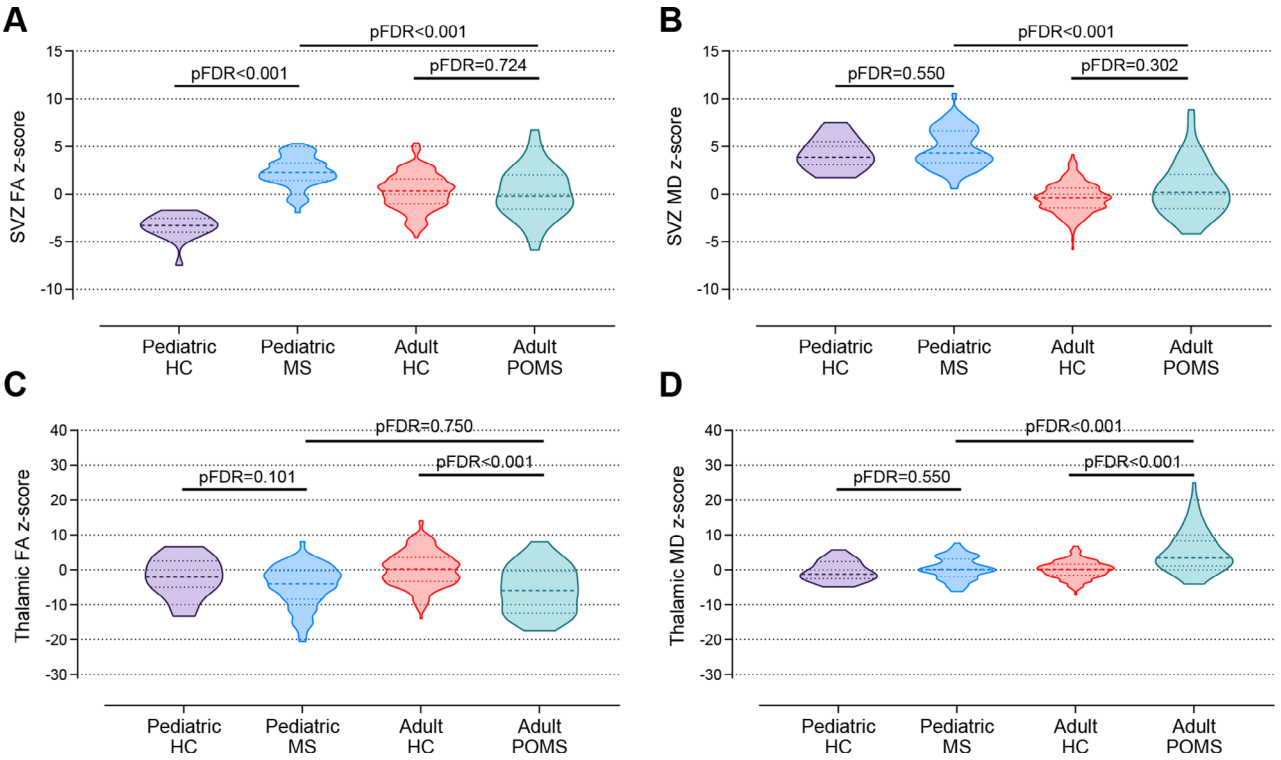


**FIGURE 3: DTI z-score distribution in pediatric multiple sclerosis and adults with pediatric-onset multiple sclerosis patients compared to their relative healthy controls. Violin plots show the distribution of FA and MD z-scores in the (A, B) subventricular zone and (C, D) thalamus, in pediatric healthy controls and pediatric multiple sclerosis and adult healthy controls and adults with pediatric-onset multiple sclerosis. FDR correction (Benjamini–Hochberg procedure) was applied. See main text and Table 3 for further details. DTI = diffusion tensor imaging; FA = fractional anisotropy; FDR = false discovery rate; HC = healthy controls; MD = mean diffusivity; MS = multiple sclerosis [Color figure can be viewed at www.annalsofneurology.org]**

and, consequently, lower MD values. Simultaneously, the organization and maturation of cellular architecture, including the alignment of migrating neuroblasts,[30] is likely to contribute to the increased FA observed in this region. As these cells differentiate, displaying a more polarized morphology, migrate, and align within the SVZ, the tissue coherence and anisotropy increase, reflecting in higher FA. These changes are essential for the proper formation and remodeling of neural circuits.[31] Over time, as these processes become less relevant, both FA and MD seem to gradually stabilize. Then, with aging, FA slightly decreases and MD slightly increases,[9] which may be attributed to increased astrogliosis, extracellular matrix deposition and loss of tissue coherence.[32,33]

Our findings observed in the thalamus are in line with previous studies[34,35] showing protracted myelination of this subcortical region into the middle age followed by gradual decline in the late adulthood. The increase in FA is largely due to progressive myelination, axonal growth, and pruning that lead to a more coherent and organized structure. The increase in MD, on the other hand, can be associated with the dynamic changes in brain tissue composition, including a progressive increase in extracellular space and water content.[34,35]

Compared to HC, FA values in the SVZ were significantly higher in patients with pediatric MS, whereas no significant differences were observed in adults with pediatric-onset MS. It is tempting to speculate that the increase of FA in the SVZ of pediatric MS patients likely reflects the complex interplay of pathological and neuroplastic processes occurring in this region (Fig 4) from the earliest phases of the disease. As observed in previous experimental studies,[14,36–38] in response to MS-related damage, mitotically active progenitor cells, subvert their physiological destiny. They migrate longitudinally along the rostral migratory stream to the olfactory bulb into areas of demyelination where they differentiate into glial cells.[39,40] Unfortunately, our results are not supported by MRI-pathological studies directly exploring the pathological substrates underlying the microstructural abnormalities of the SVZ detected with MRI in MS patients. Despite this, prior evidence may support the hypothesis that increased FA in the SVZ reflects specific physiopathological processes associated with enhanced tissue coherence and anisotropy. These processes may involve increased polarization and mobilization of newly formed cells, rather than MS-related pathological changes confined to the SVZ but absent in other brain regions.

**TABLE 4. Associations between Clinical and MRI Features with Subventricular Zone and Thalamic Region Z-Scores in Pediatric Multiple Sclerosis Patients and Adults with Pediatric-Onset Multiple Sclerosis**

| | Pediatric MS | | | | | | | | Adults with Pediatric-Onset MS | | | | | | | |
|---|---|---|---|---|---|---|---|---|---|---|---|---|---|---|---|---|
| | SVZ FA | | SVZ MD | | Thalamic FA | | Thalamic MD | | SVZ FA | | SVZ MD | | Thalamic FA | | Thalamic MD | |
| Variable | β (SE) (95% CI) | *p*-Value (pFDR) | β (SE) (95% CI) | *p*-Value (pFDR) | β (SE) (95% CI) | *p*-Value (pFDR) | β (SE) (95% CI) | *p*-Value (pFDR) | β (SE) (95% CI) | *p*-Value (pFDR) | β (SE) (95% CI) | *p*-Value (pFDR) | ββ (SE) (95% CI) | *p*-Value (pFDR) | β (SE). (95% CI) | *p*-Value (pFDR) |
| Disease duration | −0.143 (0.125) (−0.394; 0.108) | 0.259 (0.259) | 0.129 (0.132) (−0.135; 0.393) | 0.330 (0.525) | −0.138 (0.131) (−0.401; 0.125) | 0.300 (0.599) | 0.110 (0.133) (−0.157; 0.376) | 0.414 (0.829) | 0.112 (0.499) (−0.886; 1.110) | 0.823 (0.848) | −0.452 (0.446) (−1.344; 0.440) | 0.315 (0.559) | −0.161 (0.445) (−1.051; 0.728) | 0.718 (0.712) | −0.236 (0.391) (−1.019; 0.546) | 0.548 (0.722) |
| EDSS score | 0.144 (0.124) (−0.103; 0.392) | 0.248 (0.248) | −0.093 (0.131) (−0.355; 0.169) | 0.480 (0.504) | −0.117 (0.130) (−0.378; 0.143) | 0.372 (0.744) | 0.116 (0.132) (−0.148; 0.379) | 0.384 (0.799) | −0.111 (0.159) | 0.490 (0.490) | −0.030 (0.144) (−0.319; 0.258) | 0.835 (0.835) | −0.381 (0.134) (−0.649; −0.114) | **0.006 (0.018)** | 0.330 (0.118) (0.093; 0.567) | **0.007 (0.014)** |
| z-SDMT score | −0.078 (0.137) (−0.353; 0.198) | 0.574 (0.574) | −0.180 (0.141) (−0.463; 0.102) | 0.205 (0.616) | 0.246 (0.140) (−0.034; 0.527) | 0.084 (0.251) | −0.129 (0.138) (−0.406; 0.148) | 0.355 (0.355) | −0.245 (0.129) (−0.503; 0.012) | 0.061 (0.183) | −0.302 (0.113) (−0.527; −0.076) | **0.010 (0.019)** | 0.304 (0.111) (0.081; 0.527) | **0.008 (0.017)** | −0.328 (0.095) (−0.518; −0.138) | **0.001 (0.002)** |
| Brain T2-hyperintense WM LV[a] | 0.006 (0.003) (0.001; 0.012) | **0.023 (0.047)** | 0.038 (0.013) (0.011; 0.065) | **0.006 (0.019)** | −0.016 (0.005) (−0.025; −0.007) | **0.001 (0.003)** | 0.152 (0.031) (0.089; 0.214) | **<0.001 (<0.001)** | −0.001 (0.002) (−0.005; 0.003) | 0.672 (0.785) | 0.026 (0.007) (0.013; 0.040) | **<0.001 (0.001)** | −0.009 (0.002) (−0.013; −0.005) | **<0.001 (<0.001)** | 0.122 (0.017) (0.087; 0.156) | **<0.001 (<0.001)** |
| NBV [$\times 10^{-3}$] | 1.762 (0.002) (−2.981; 4.560) | 0.461 (0.461) | −0.889 (0.009) (−1.123; 0.092) | **<0.001 (<0.001)** | 0.221 (0.003) (−0.817; 0.463) | **<0.001 (<0.001)** | −1.853 (0.201) (−2.059; −1.523) | **<0.001 (<0.001)** | 0.004 (0.003) (−0.100; 0.026) | 0.244 (0.733) | −0.378 (0.105) (−0.588; −0.169) | **0.001 (0.002)** | 0.120 (0.003) (0.061; 0.181) | **<0.001 (0.001)** | −1.189 (0.897) (−2.422; −1.382) | **<0.001 (<0.001)** |
| Normalized thalamic volume | −0.023 (0.124) (−0.270; 0.225) | 0.853 (0.853) | −0.410 (0.118) (−0.647; −0.174) | **0.001 (0.003)** | 0.566 (0.106) (0.354; 0.778) | **<0.001 (<0.001)** | −0.568 (0.107) (−0.783; −0.353) | **<0.001 (<0.001)** | −0.056 (0.158) (−0.371; 0.260) | 0.725 (0.725) | −0.447 (0.130) (−0.708; −0.186) | **0.001 (0.003)** | 0.604 (0.119) (0.365; 0.843) | **<0.001 (<0.001)** | −0.635 (0.093) (−0.822; −0.449) | **<0.001 (<0.001)** |
| Normalized caudate volume | −0.180 (0.134) (−0.448; 0.089) | 0.186 (0.372) | −0.284 (0.138) (−0.560; −0.008) | **0.044** (0.133) | 0.431 (0.131) (0.169; 0.693) | **0.002 (0.007)** | −0.463 (0.131) (−0.725; −0.202) | **0.001 (0.002)** | −0.015 (0.162) (−0.340; 0.309) | 0.925 (0.925) | −0.398 (0.137) (−0.674; −0.123) | **0.005 (0.016)** | 0.424 (0.136) (0.151; 0.697) | **0.003 (0.009)** | −0.484 (0.112) (−0.708; −0.260) | **<0.001 (<0.001)** |
| Normalized CP volume | 0.005 (0.002) (0.002; 0.008) | **0.001 (0.004)** | 0.011 (0.008) (−0.006; 0.028) | 0.203 (0.321) | −0.012 (0.003) (−0.017; −0.007) | **<0.001 (<0.001)** | 0.061 (0.021) (0.020; 0.102) | **0.004 (0.013)** | −0.001 (0.003) (−0.007; 0.006) | 0.870 (0.870) | 0.022 (0.011) (0.001; 0.044) | 0.041 (0.082) | −0.012 (0.003) (−0.018; −0.006) | **<0.001 (<0.001)** | 0.122 (0.030) (0.062; 0.182) | **<0.001 (<0.001)** |

Standardized beta coefficients (β), related standard errors (SE), and *p* values from age- and sex-adjusted linear models are reported. Bold values denote statistical significance ($p < 0.05$). MD is expressed in units of $mm^2/s \times 10^{-3}$. FA is a dimensionless index.

CI = confidence interval; CP = choroid plexus; EDSS = Expanded Disability Status Scale; FA = fractional anisotropy; pFDR = false discovery rate p value; LV = lesion volume; MD = mean diffusivity; MS = multiple sclerosis; NBV = normalized brain volume; SDMT = Symbol Digit Modalities Test; SE = standard error; WM = white matter.

[a]T2-hyperintense WM LV was log transformed.

Previous combined MRI-pathological studies investigating various brain regions have shown that processes influencing tissue coherence and anisotropy can substantially influence FA. For example, in the cortex, anisotropy is strongly influenced by the structural organization of projective axons, horizontal fibers, and dendritic arborizations. Projective axons contribute to higher anisotropy—and consequently high FA values—through their high directional coherence, myelination, and their role in promoting an orientation orthogonal to the cortical surface of the major diffusion tensor eigenvector.[41–43] Conversely, horizontal fibers and dendritic arborizations decrease anisotropy by branching extensively in multiple directions, which increases the isotropic diffusion component and reduces tissue coherence. Consistent with this, studies on brain development[41,42] have shown that at 26 weeks of gestational age, the human fetal cortex exhibits high FA values. At this stage, cortical maturation—including the development of dendritic arborizations, synapses, and afferent fibers—has not yet occurred, resulting in highly

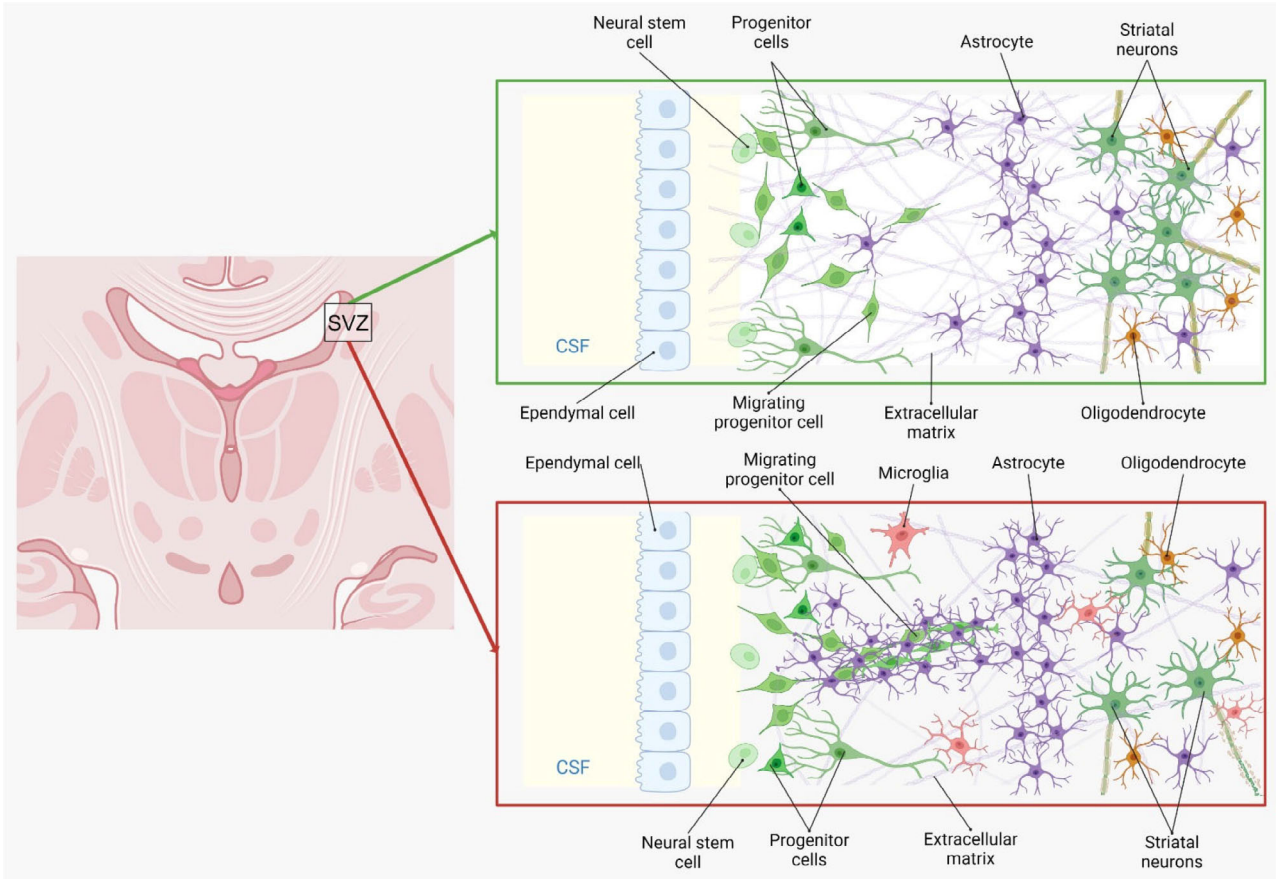


**FIGURE 4: Representations of the subventricular zone in the normal brain and of the possible changes occurring in multiple sclerosis. The subventricular zone is located directly beneath the ependymal layer on the lateral wall of the lateral ventricles. The control subventricular zone (green box) is composed of a ribbon of astrocytes separated from the ependymal wall by a hypocellular gap, containing few early progenitors. In multiple sclerosis subventricular zone (red box), the density of astrocytes and early progenitors is increased. The presence of progenitors with a bipolar morphology suggests their potential migration away from the subventricular zone. SVZ = subventricular zone [Color figure can be viewed at www.annalsofneurology.org]**

anisotropic tissue with the main eigenvector oriented perpendicular to the cortical surface. Interestingly, the loss of projective axons in the normal-appearing cortex of MS patients is associated with reduced FA.[44–46] However, in demyelinated cortex, the simultaneous loss of projective axons, horizontal fibers, and dendrites may paradoxically increase tissue coherence, leading to higher FA values in MS-demyelinated cortex.[44,45]

Moreover, supporting these hypotheses, a neuropathological study detected a 2- to 3-fold increase in cell density and proliferation in the SVZ of postmortem MS brains compared with non-neurological controls.[47] Most interestingly, progenitors were detected in demyelinated MS lesions, especially those located periventricularly, suggesting a mobilization of SVZ-derived early glial progenitors to periventricular lesions, where they could give rise to oligodendrocyte precursors.[47] Another study investigating subcortical chronic MS lesions detected a population of newborn neurons, functionally differentiated and integrated within local networks by synapse formation, which may have originated from neural progenitor cells in the adjacent SVZ.[48]

However, although there is growing evidence that endogenous neurogenesis and gliogenesis contribute to self-repair in inflammatory central nervous system (CNS) disorders, the endogenous stem cell compartment often fails to achieve complete and lasting repair.[6] As the disease progresses, these processes are likely to diminish over time,[49] which may explain the lack of significance we observed in adults with pediatric-onset MS patients compared to HC. Indeed, we may hypothesize that, in adults, the physiological decline of SVZ properties due to aging is compounded by the pathological processes occurring in MS, which tend to dominate over reparative mechanisms. Consequently, while reparative processes may still be present, they are counteracted by these pathological mechanisms, creating a dual dynamic.

On the other side, while no differences were observed in MD SVZ in both pediatric MS and adults

with pediatric-onset MS compared to their counterpart HC, adults with pediatric-onset MS showed higher MD values compared to pediatric MS. The increase in MD might indicate a breakdown of barriers, such as myelin or cellular membranes, and more free water movement in the SVZ. This could be due either to inflammation-induced edema or extracellular matrix degradation or damage to neural progenitor cells. Previous experimental studies demonstrated that inflammatory changes influence the subventricular niche composition and functionality, possibly impairing neural precursors' by-stander effect.[6,50] Interestingly, our findings are consistent with a previous study, showing higher MD values in patients having a longer disease duration.[16] Recent data suggest that this failure may be due to the influence of inflammatory components, such as infiltrating blood-borne mononuclear cells, reactive CNS-resident cells (like astrocytes, brain endothelial cells, and microglia), and humoral mediators (including cytokines and chemokines).[6] These factors can impact the proliferation and differentiation of adult neural progenitor cells by directly or indirectly disrupting their developmental genetic programs.[6,49] Moreover, the degradation of the extracellular matrix can compromise the polarity (thus lowering the FA) of the SVZ and negatively affecting the maturation and migration of stem cell precursors, particularly in the advanced stages of MS. Therefore, it is tempting to speculate that, in more advanced phases of the disease, 2 processes could occur simultaneously, which potentially have opposite effects on microstructural characteristics (stemness vs MS-related damage).

To further test our hypotheses and support the specificity of our findings in the SVZ, we evaluated a control region represented by the thalamus. Interestingly, even though the thalamus has a topographic location similar to the SVZ, being bathe from the CSF, the patterns of microstructural abnormalities of these 2 structures were different throughout the disease course, supporting the uniqueness of the SVZ. This could indicate the presence of neuroplasticity mechanisms in this region not detectable in the thalamus. Indeed, no significant differences in thalamic FA and MD values were observed in pediatric MS. Conversely, in adults with pediatric-onset MS significantly lower FA and higher MD values were observed compared to adult HC. Our findings are in line with previous studies performed in MS patients applying different MRI techniques[51,52] and showing microstructural damage in the band closest to the CSF.

To better explore the possible mechanisms occurring in the SVZ and in the thalamus, we evaluated their association with choroid plexus volume. The CSF, whose composition is mainly determined by the choroid plexus secretome, is a major source of proteins and smaller molecules that signal the SVZ.[53] Notably, inflammatory stimuli, such as lipopolysaccharide injection, has been demonstrated to determine acute and transient changes in the choroid plexus transcriptome, affecting CSF composition.[54] Such alterations may transiently impact the SVZ niche population, as observed in developmental studies where maternal peripheral inflammation influenced fetal ventricular zone proliferation and cortical layer formation.[55] Interestingly, while we observed significant association between choroid plexus volume with thalamic FA both in pediatric MS and adults with pediatric-onset MS, an association with SVZ FA was found only in the pediatric MS cohort. It is tempting to speculate that heterogeneous pathophysiological processes may occur in these 2 regions. In the thalamus, the chronic pro-inflammatory state associated with choroid plexus enlargement and CSF may be associated with gradual and progressive thalamic demyelination and neuro-axonal damage. At the level of the SVZ, the bout of inflammation observed in the first phases of the disease and characterized by the presence of pro-inflammatory cytokines in the CSF may initially trigger proliferation and migration of progenitor cells. This is supported by the evidence of a significant association between higher SVZ FA and higher choroid plexus volume in pediatric MS patients but also with a higher T2 LV. In more advanced phases of the disease, these plasticity processes become exhausted[49] and neurodegenerative processes become predominant.

Regarding the clinical relevance of these metrics, according to previous studies,[56,57] we observed associations between lower thalamic FA and higher thalamic MD with higher EDSS score and T2 LV as well as with lower z-SDMT score and brain volumes both in pediatric MS and in adults with pediatric-onset MS, confirming that damage of periventricular regions is associated with disability and structural damage.[51,58] The lack of associations of SVZ FA with disease duration, EDSS score, z-SDMT score in pediatric MS may be due to the simultaneous influence of different processes that could affect DTI measures in opposite directions. These include neuroplasticity and MS-related damage accumulation, which may ultimately result into the preservation of clinical function.[49] Interestingly, higher SVZ MD was significantly associated with lower z-SDMT score in adults with pediatric-onset MS. Although a causative role of SVZ in supporting cognitive function has not been demonstrated yet, our findings align with a previous study[15] showing an impaired homeostasis in cognitive processes in patients with pathological SVZ damage.

On the other hand, in line with the hypothesis of an increased SVZ MD due to increased extracellular space in

response to damage, we observed associations between this metric and higher T2 WM LV, lower NBV, normalized thalamic and caudate volumes in adults with pediatric-onset MS.

This study has some limitations. First, it is cross-sectional, and we cannot speculate any causal relation between the different measures analyzed. Second, due to the difficulty in the enrolment of pediatric healthy subjects in MRI studies, we included 22 pediatric HC, potentially limiting the extent of normal variability in quantitative MRI metrics, especially in developing subjects. Third, our findings may be influenced by partial volume effect due to brain volume loss and proximity to the ventricle. However, partial volume typically reduces average FA values, whereas our results showed increased FA in the SVZ of pediatric MS patients. Additionally, the absence of significant MD variations confirms minimal contamination from the ventricular front. Finally, we carefully controlled this aspect by applying a threshold during the registration of the SVZ mask from 3D T1-weighted sequence to diffusion space and, as performed in a previous study,[25] by comparing the results with those from the thalamic region, which has similar anatomical localization. Fourth, considering the potential relevance of the SVZ in MS, MRI-pathological studies are needed to confirm and expand our findings. Finally, although DTI is sensitive to detect MS-related damage, it lacks specificity in distinguishing between the different pathological substrates. Future studies including a longitudinal assessment, should evaluate the SVZ dynamics by applying more advanced MRI techniques (eg, neurite orientation dispersion and density imaging).

In conclusion, in HC we observed a simultaneous increase of FA and decrease of MD in the SVZ with aging, possibly reflecting cell differentiation and migration along with increased cell density. Compared to HC, pediatric MS showed higher FA in the SVZ, with this metric decreasing as disease duration increased. This may indicate a gradual exhaustion of reparative mechanisms, partially due to MS-related damage. Altogether, our findings suggest that SVZ microstructural changes are an early phenomenon in the pathophysiology of pediatric MS, and associate with brain structural damage but not with clinical impairment.

## Author Contributions

M.M., M.F., and M.A.R. contributed to the conception and design of the study. M.M., L.S., E.P., P.P, D.M., M.G., M.R., L.M., M.F., and M.A.R. contributed to the acquisition and analysis of data. M.M., L.S., E.P., P.P, D.M., M.G., M.R., L.M., M.F., and M.A.R. contributed to drafting the text and preparing the figures. M.M., L.S., E.P., P.P, D.M., M.G., M.R., L.M., M.F., and M.A.R. approved the final draft of the manuscript.

## Potential Conflicts of Interest

Nothing to report.

### *Data availability*

The anonymized dataset used and analyzed during the current study is available from the corresponding author upon reasonable request.

## References


1. Fadda G, Armangue T, Hacohen Y, et al. Paediatric multiple sclerosis and antibody-associated demyelination: clinical, imaging, and biological considerations for diagnosis and care. Lancet Neurol 2021;20:136–149.
2. Margoni M, Preziosa P, Rocca MA, Filippi M. Pediatric multiple sclerosis: developments in timely diagnosis and prognostication. Expert Rev Neurother 2022;22:393–403.
3. McKay KA, Manouchehrinia A, Berrigan L, et al. Long-term cognitive outcomes in patients with pediatric-onset vs adult-onset multiple sclerosis. JAMA Neurol 2019;76:1028–1034.
4. Luskin MB. Restricted proliferation and migration of postnatally generated neurons derived from the forebrain subventricular zone. Neuron 1993;11:173–189.
5. Curtis MA, Faull RL, Eriksson PS. The effect of neurodegenerative diseases on the subventricular zone. Nat Rev Neurosci 2007;8:712–723.
6. Martino G, Pluchino S. The therapeutic potential of neural stem cells. Nat Rev Neurosci 2006;7:395–406.
7. Sanai N, Nguyen T, Ihrie RA, et al. Corridors of migrating neurons in the human brain and their decline during infancy. Nature 2011;478:382–386.
8. Coletti AM, Singh D, Kumar S, et al. Characterization of the ventricular-subventricular stem cell niche during human brain development. Development 2018;145:145.
9. Conover JC, Shook BA. Aging of the subventricular zone neural stem cell niche. Aging Dis 2011;2:49–63.
10. David-Bercholz J, Kuo CT, Deneen B. Astrocyte and oligodendrocyte responses from the subventricular zone after injury. Front Cell Neurosci 2021;15:797553.
11. Nait-Oumesmar B, Picard-Riera N, Kerninon C, Baron-Van EA. The role of SVZ-derived neural precursors in demyelinating diseases: from animal models to multiple sclerosis. J Neurol Sci 2008;265:26–31.
12. Etxeberria A, Mangin JM, Aguirre A, Gallo V. Adult-born SVZ progenitors receive transient synapses during remyelination in corpus callosum. Nat Neurosci 2010;13:287–289.
13. Samanta J, Grund EM, Silva HM, et al. Inhibition of Gli1 mobilizes endogenous neural stem cells for remyelination. Nature 2015;526:448–452.
14. Butti E, Bacigaluppi M, Chaabane L, et al. Neural stem cells of the subventricular zone contribute to neuroprotection of the corpus callosum after cuprizone-induced demyelination. J Neurosci 2019;39:5481–5492.
15. Butti E, Cattaneo S, Bacigaluppi M, et al. Neural precursor cells tune striatal connectivity through the release of IGFBPL1. Nat Commun 2022;13:7579.
16. Cellerino M, Schiavi S, Lapucci C, et al. In-vivo characterization of macro- and microstructural injury of the subventricular zone in relapsing-remitting and progressive multiple sclerosis. Front Neurosci 2023;17:1112199.
17. Liu LL, Shannahan J, Zheng W. Choroid plexus modulates subventricular zone adult neurogenesis and olfaction through secretion of small extracellular vesicles. bioRxiv 2023.

18. Thompson AJ, Banwell BL, Barkhof F, et al. Diagnosis of multiple sclerosis: 2017 revisions of the McDonald criteria. Lancet Neurol 2018;17:162–173.
19. Portaccio E, Goretti B, Lori S, et al. The brief neuropsychological battery for children: a screening tool for cognitive impairment in childhood and juvenile multiple sclerosis. Mult Scler 2009;15:620–626.
20. Tedone N, Vizzino C, Meani A, et al. The brief repeatable battery of neuropsychological tests (BRB-N) version a: update of Italian normative data from the Italian neuroimaging network initiative (INNI). J Neurol 2024;271:1813–1823.
21. Battaglini M, Jenkinson M, De Stefano N, Alzheimer's Disease Neuroimaging I. SIENA-XL for improving the assessment of gray and white matter volume changes on brain MRI. Hum Brain Mapp 2018; 39:1063–1077.
22. Patenaude B, Smith SM, Kennedy DN, Jenkinson M. A Bayesian model of shape and appearance for subcortical brain segmentation. NeuroImage 2011;56:907–922.
23. Andersson JLR, Graham MS, Drobnjak I, et al. Towards a comprehensive framework for movement and distortion correction of diffusion MR images: within volume movement. NeuroImage 2017;152:450–466.
24. Schilling KG, Blaber J, Huo Y, et al. Synthesized b0 for diffusion distortion correction (Synb0-DisCo). Magn Reson Imaging 2019;64: 62–70.
25. Cherubini A, Spoletini I, Peran P, et al. A multimodal MRI investigation of the subventricular zone in mild cognitive impairment and Alzheimer's disease patients. Neurosci Lett 2010;469:214–218.
26. Margoni M, Gueye M, Meani A, et al. Choroid plexus enlargement in paediatric multiple sclerosis: clinical relevance and effect of sex. J Neurol Neurosurg Psychiatry 2023;94:181–188.
27. Lebel C, Beaulieu C. Longitudinal development of human brain wiring continues from childhood into adulthood. J Neurosci 2011;31: 10937–10947.
28. Lebel C, Walker L, Leemans A, et al. Microstructural maturation of the human brain from childhood to adulthood. NeuroImage 2008; 40:1044–1055.
29. Niimi Y, Levison SW. Pediatric brain repair from endogenous neural stem cells of the subventricular zone. Pediatr Res 2018;83:385–396.
30. Alvarez-Buylla A, Garcia-Verdugo JM. Neurogenesis in adult subventricular zone. J Neurosci 2002;22:629–634.
31. Bacigaluppi M, Sferruzza G, Butti E, et al. Endogenous neural precursor cells in health and disease. Brain Res 2020;1730:146619.
32. Statzer C, Park JYC, Ewald CY. Extracellular matrix dynamics as an emerging yet understudied Hallmark of aging and longevity. Aging Dis 2023;14:670–693.
33. Volterra A, Meldolesi J. Astrocytes, from brain glue to communication elements: the revolution continues. Nat Rev Neurosci 2005;6: 626–640.
34. Arshad M, Stanley JA, Raz N. Adult age differences in subcortical myelin content are consistent with protracted myelination and unrelated to diffusion tensor imaging indices. NeuroImage 2016;143:26–39.
35. Little G, Acosta-Franco JA, Beaulieu C. Automated surface-based segmentation of deep gray matter regions based on diffusion tensor images reveals unique age trajectories over the healthy lifespan, bioRxiv 2023:2023.2010.2004.560912.
36. Gonzalez-Perez O, Alvarez-Buylla A. Oligodendrogenesis in the subventricular zone and the role of epidermal growth factor. Brain Res Rev 2011;67:147–156.
37. Menn B, Garcia-Verdugo JM, Yaschine C, et al. Origin of oligodendrocytes in the subventricular zone of the adult brain. J Neurosci 2006;26:7907–7918.
38. Xing YL, Roth PT, Stratton JA, et al. Adult neural precursor cells from the subventricular zone contribute significantly to oligodendrocyte regeneration and remyelination. J Neurosci 2014;34:14128–14146.
39. Brundin L, Brismar H, Danilov AI, et al. Neural stem cells: a potential source for remyelination in neuroinflammatory disease. Brain Pathol 2003;13:322–328.
40. Picard-Riera N, Decker L, Delarasse C, et al. Experimental autoimmune encephalomyelitis mobilizes neural progenitors from the subventricular zone to undergo oligodendrogenesis in adult mice. Proc Natl Acad Sci USA 2002;99:13211–13216.
41. McKinstry RC, Mathur A, Miller JH, et al. Radial organization of developing preterm human cerebral cortex revealed by non-invasive water diffusion anisotropy MRI. Cereb Cortex 2002;12:1237–1243.
42. Ouyang M, Dubois J, Yu Q, et al. Delineation of early brain development from fetuses to infants with diffusion MRI and beyond. NeuroImage 2019;185:836–850.
43. Miller KL, Stagg CJ, Douaud G, et al. Diffusion imaging of whole, post-mortem human brains on a clinical MRI scanner. NeuroImage 2011;57:167–181.
44. Preziosa P, Kiljan S, Steenwijk MD, et al. Axonal degeneration as substrate of fractional anisotropy abnormalities in multiple sclerosis cortex. Brain 2019;142:1921–1937.
45. Jonkman LE, Klaver R, Fleysher L, et al. The substrate of increased cortical FA in MS: a 7T post-mortem MRI and histopathology study. Mult Scler 2016;22:1804–1811.
46. Jurgens T, Jafari M, Kreutzfeldt M, et al. Reconstruction of single cortical projection neurons reveals primary spine loss in multiple sclerosis. Brain 2016;139:39–46.
47. Nait-Oumesmar B, Picard-Riera N, Kerninon C, et al. Activation of the subventricular zone in multiple sclerosis: evidence for early glial progenitors. Proc Natl Acad Sci USA 2007;104:4694–4699.
48. Chang A, Smith MC, Yin X, et al. Neurogenesis in the chronic lesions of multiple sclerosis. Brain 2008;131:2366–2375.
49. Pluchino S, Muzio L, Imitola J, et al. Persistent inflammation alters the function of the endogenous brain stem cell compartment. Brain 2008;131:2564–2578.
50. Pourabdolhossein F, Gil-Perotin S, Garcia-Belda P, et al. Inflammatory demyelination induces ependymal modifications concomitant to activation of adult (SVZ) stem cell proliferation. Glia 2017;65: 756–772.
51. Rubin M, Pagani E, Preziosa P, et al. Cerebrospinal fluid-in gradient of cortical and deep gray matter damage in multiple sclerosis. Neurol Neuroimmunol Neuroinflamm 2024;11:e200271.
52. Pardini M, Brown JWL, Magliozzi R, et al. Surface-in pathology in multiple sclerosis: a new view on pathogenesis? Brain 2021;144: 1646–1654.
53. Falcao AM, Marques F, Novais A, et al. The path from the choroid plexus to the subventricular zone: go with the flow! Front Cell Neurosci 2012;6:34.
54. Marques F, Sousa JC, Coppola G, et al. Kinetic profile of the transcriptome changes induced in the choroid plexus by peripheral inflammation. J Cereb Blood Flow Metab 2009;29:921–932.
55. Stolp HB, Turnquist C, Dziegielewska KM, et al. Reduced ventricular proliferation in the foetal cortex following maternal inflammation in the mouse. Brain 2011;134:3236–3248.
56. Mesaros S, Rocca MA, Pagani E, et al. Thalamic damage predicts the evolution of primary-progressive multiple sclerosis at 5 years. AJNR Am J Neuroradiol 2011;32:1016–1020.
57. Schoonheim MM, Hulst HE, Brandt RB, et al. Thalamus structure and function determine severity of cognitive impairment in multiple sclerosis. Neurology 2015;84:776–783.
58. Magliozzi R, Fadda G, Brown RA, et al. "ependymal-in" gradient of thalamic damage in progressive multiple sclerosis. Ann Neurol 2022; 92:670–685.